Patient-specific in-vivo QA in MRGRT: 3D EPID dosimetry for the Unity MR-linac

Torres Xirau, I.

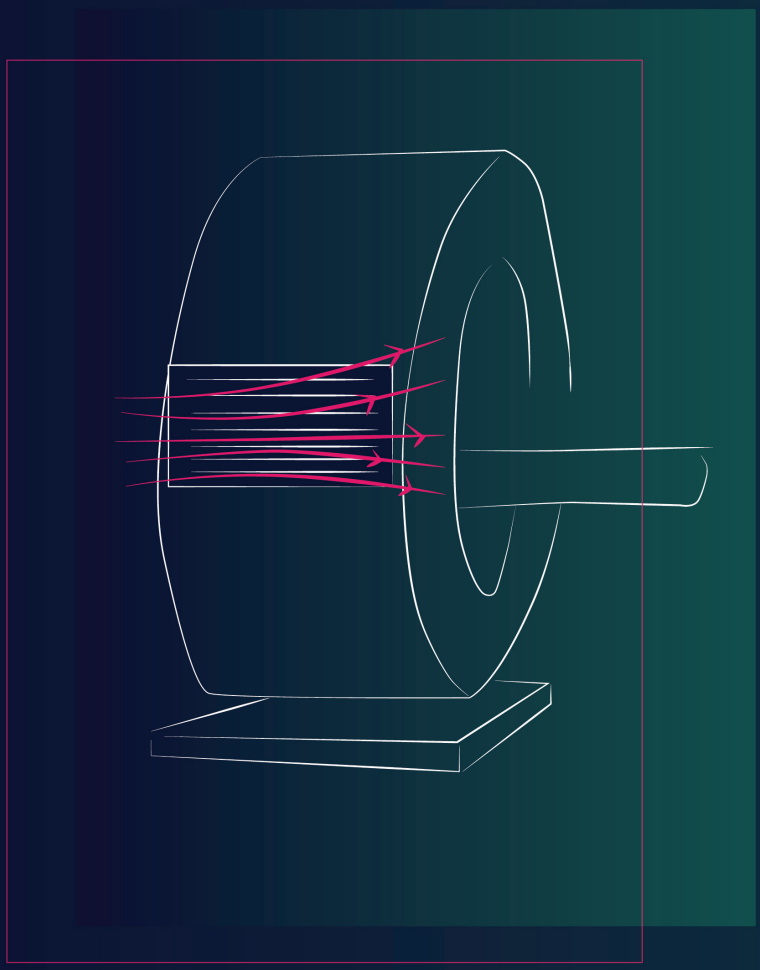

3.

A BACK-PROJECTION ALGORITHM IN THE PRESENCE OF AN EXTRA ATTENUATING MEDIUM: TOWARDS EPID DOSIMETRY FOR THE MR-LINAC

I Torres-Xirau
I Olaciregui-Ruiz
R A Rozendaal
P González
B J Mijnheer
J-J Sonke
U A van der Heide
A Mans

Department of Radiation Oncology,
The Netherlands Cancer Institute–Antoni van Leeuwenhoek Hospital,
Plesmanlaan 121, 1066 CX Amsterdam, The Netherlands

Physics in Medicine & Biology, Volume 62, Number 15
Published 17 July 2017 •

Abstract

Electronic portal imaging devices (EPIDs) are frequently used in external beam radiation therapy for dose verification purposes. The aim of this study was to investigate the dose-response characteristics of the EPID in the Unity MR-linac (Elekta AB, Stockholm, Sweden) relevant for dosimetric applications under clinical conditions. EPID images and ionization chamber measurements were used to study the effects of the magnetic field, the scatter generated in the MR housing reaching the EPID, and inhomogeneous attenuation from the MR housing. Dose linearity and dose rate dependencies were also determined.

The magnetic field strength at EPID level did not exceed 10 mT, and dose linearity and dose rate dependencies proved to be comparable to that on a conventional linac. Profiles of fields, delivered with and without the magnetic field, were indistinguishable. The EPID center had an offset of 5.6 cm in the longitudinal direction, compared to the beam central axis, meaning that large fields in this direction will partially fall outside the detector area and not be suitable for verification. Beam attenuation by the MRI scanner and the table is gantry angle dependent, presenting a minimum attenuation of 67% relative to the 90° measurement. Repeatability, observed over 2 months, was within 0.5% (1 SD).

In order to use the EPID for dosimetric applications in the MR-linac, challenges related to the EPID position, scatter from the MR housing, and the inhomogeneous, gantry angle-dependent attenuation of the beam will need to be solved.

Keywords: EPID, dosimetry, MR-linac, QA, Unity.

3.1. Introduction

Electronic portal imaging devices (EPIDs), although originally intended for patient position verification, are increasingly being utilized for dosimetric applications, both for pre-treatment and *in vivo* dose verification. The amorphous silicon (a-Si) EPIDs mounted on conventional linacs have been extensively studied and have shown dose-response characteristics suitable for dose verification [111–115,127–129]. The use of EPIDs for dosimetric purposes is already clinical routine [88,90,130–132].

One of the most interesting advancements in radiotherapy in recent years is the introduction of machines that combine a radiation source with an MRI system. The Elekta MR-linac system [92] is equipped with an EPID, mounted on the rotating gantry, opposite to the accelerator head. This allows for simultaneous EPID acquisition and MR imaging [93].

The integration of a linac and an MRI system, combined with emerging techniques for fast re-contouring and re-planning, is expected to make online adaptive strategies a feasible technique in the clinic [94]. The complexity of these techniques and of the newly developed MR-linac makes independent patient-specific dosimetric verification and quality assurance (QA) highly desirable.

EPID dosimetry has proven to be a valuable technique to identify errors related not only to data transfer, dose delivery, and patient set-up, but also to MLC calibration and to dose calculation [105]. An intrinsic advantage of EPIDs is that they allow for dose verification in real-time [89,133]. Within the framework of the MR-linac, where a different plan is generated and delivered every day, transit EPID dosimetry could provide an independent real-time verification of the entire treatment chain.

The purpose of this work was to examine the challenges related to the implementation of EPID-based dosimetric applications in the MR-linac. The presence of the MRI housing between the patient and the EPID acts as a secondary source of scatter and attenuates the primary beam. Also, the magnetic field causes an electron return effect on the secondary scattered electrons, both inside the bore and at the EPID level. The relative position of the panel in the system, the gantry angle dependence of the EPID signal, the EPID response to the MRI scatter and the pixel sensitivity variation with and without magnetic field were examined in this work. The panel repeatability, EPID ghosting, linearity and dose rate dependence of the panel were also studied.

A practical approach towards the development of an EPID dosimetry method for the MR-linac would be to adapt existing EPID solutions for conventional linacs. For this sake, and whenever applicable, the characteristics of the EPID in the MR-linac are compared to those in conventional linacs.

3.2. Materials and Methods

MR-linac, EPID, and acquisition software

The Unity MR-linac system consists of a linac (Elekta AB, Stockholm, Sweden) with a nominal 7 MV flattening filter free (FFF) beam and an integrated wide bore 1.5 T MRI scanner (Philips Medical Systems, Best, the Netherlands). The system is equipped with a multi-leaf collimator (MLC) consisting of 160 leaves with a projected width of a single leaf of 0.72 cm at the isocenter plane.

A ring gantry, on which the accelerator and EPID are mounted, is built around the MRI scanner, with the EPID opposite to the accelerator. In the geometry of the MR-linac, the source-to-isocenter distance is

143.5 cm, and the source-to-detector distance (SDD) is fixed to 263.5 cm, yielding to a magnification factor of 1.84. The maximum field size achievable with this MLC is 57 x 22 cm^2 at the isocenter.

To minimize beam attenuation and obtain homogeneous transmission towards the isocenter, the central region (along the longitudinal direction) of the magnet is free of gradient coils and shimming hardware (Figure 1). A pipe in the MR scanner connecting the split coils is located at a gantry angle of 13° and the system does not allow the use of leaf pair/gantry combinations that cause direct irradiation to the pipe. The gap also limits the acquisition of un-attenuated beams to an irradiation field of a maximum of ±4.8 cm in each direction of the longitudinal axis at the isocenter. For larger fields, the exit beam's dimensions exceed the coil-free region and therefore, the beam is inhomogeneously attenuated at the EPID level.

The Elekta iViewGT panel is an a-Si flat panel X-ray detector (XRD 1642 AP, Perkin Elmer Optoelectronics, Wiesbaden, Germany) with a 41x41 cm^2 detection area (1024x1024 pixels), with a pixel pitch of 0.4 mm. The integrated images were acquired using Elekta's iViewGT software (5.0.0). Frames were acquired with a frame integration time of 285 ms (3.5 fps). EPID movies were acquired with the XIS software (Perkin Elmer) with 266 ms frame integration time (3.7 fps). Single level gain calibration, bad pixel map and offset (dark current) correction were applied to all images. No saturation issues were experienced during the acquisition, given the fact that at the MR-Linac the panel is at a greater distance from the source and in addition there is a lot of extra attenuation, the panel therefore sees a very low dose rate compared to the dose rate of a panel in a standard linac with FFF beams.

Measurements for comparison to a conventional linac were performed using a 6 MV flattened photon beam of an SL20i linear accelerator

(Elekta AB, Stockholm, Sweden), equipped with a multileaf collimator (MLC) of 80 leafs with a projected leaf width of 1 cm at the isocenter, which is located 100 cm from the target. An Elekta iViewGT a-Si EPID (PerkinElmer RID 1640 AL5) was used at 60 cm from the isocenter.

In this work, the EPID output was calculated by averaging the signal received by the EPID on the on-axis region of 10x10 pixels (4x4 mm^2 at the EPID level). Unless explicitly mentioned, measurements in the MR-linac were performed with the magnetic field on, and all field sizes refer to the isocenter plane. As only relative measurements were performed using ionization chambers, array detectors and microDiamond detectors, no correction factors were required to account for effects of the magnetic field [134,135].

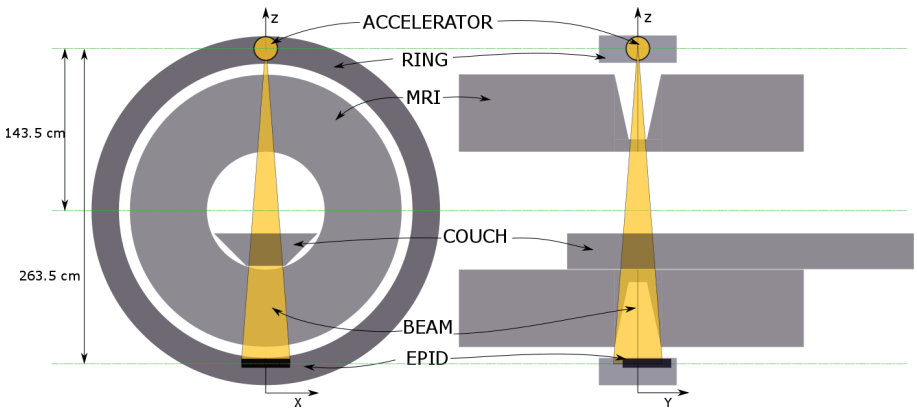

Figure 3.1. MR-linac cross-sections. In the Y-Z plane, the beam center is not aligned with the center of the panel (black box), so parts of large fields will fall outside the EPID detection area.

EPID relative position and MRI scanner

Due to mechanical constraints, the EPID is mounted in a fixed position and its center is not aligned to the center of the beam in the longitudinal direction (Y-direction in **Figure 3.1**). To measure the displacement of the EPID, square fields of sizes ranging from 2x2 to 8x8 cm^2 of 200 MU

were used to irradiate the EPID and images were acquired. Borders of the fields were detected by an edge detection algorithm and the average offset for all images was determined.

The mechanical flex of the EPID in the MR-linac was calculated by irradiating a 5x5 cm^2 field every 5 degrees and the field edge tracked on the EPID images to measure the lateral displacement.

EPID response to scatter from the MRI scanner

To study the effect of scatter from the MRI scanner on EPID images, microDiamond detector (PTW, Freiburg, Germany) measurements were performed at the EPID level and compared with portal images acquired for fields of increasing sizes (2x2 - 22x22 cm^2) irradiated with 200 MU at gantry 0°. The results, normalized to the 10x10 cm^2 measurement, were also compared to those from a conventional linac. A brass build-up cap was used to perform the microDiamond detector measurements on top of the EPID, and its position was aligned to the center of the beam using EPID images.

Angular dependence of the beam attenuation at isocenter and EPID level

With the design of the non-clinical prototype, structures of the couch, as well as structures in the MRI scanner, cause high attenuation of the beam at several gantry angles. This needs to be taken into account by the treatment planning system for delivery, but also when characterizing the response of the EPID for dosimetric purposes.

The dose at the isocenter was compared to the EPID signal. A Farmer-type ionization chamber (IC) (NE2571, Phoenix Dosimetry Ltd, Sandhurst, UK) in a homemade 20 cm diameter cylindrical PMMA phantom was used to acquire the angular output dependency of the

beam. The phantom was isocentrically aligned using two orthogonal EPID images. Readings were acquired for every 5 degrees, and every degree for regions with high gradient in attenuation. EPID images were acquired without the phantom in the beam, using a 10x10 cm^2 field, at the same angles as for the Farmer chamber measurements.

The angles 7-19 degrees were excluded from the study, as they are prohibited for 10x10 cm^2 fields due the pipe at 13°.

EPID response with and without magnetic field

In the presence of a magnetic field, the so-called electron return effect (ERE) occurs at interfaces between media with different electron densities. The ERE has been a subject of study within the MR-linac community for its role in dose redistributions at tissue-air boundaries [91,117,136]. The ERE also affects scattered electrons, originating from the MRI housing between the isocenter and the EPID, the ring where the EPID is mounted, or within the EPID itself.

A 20 cm thick slab phantom was irradiated with square fields with sizes varying from 2x2 to 20x20 cm^2 using 200MU and EPID images were acquired, both with and without the magnetic field. The images with the magnetic field on were acquired one month after those with the field off. In that time, the EPID was recalibrated. Therefore, images acquired without the magnetic field were normalized to their counterpart in field-size with the magnetic field and compared by means of a 2D γ-analysis (local, 2%, 1mm, 50% isodose region) and X and Y lateral profiles were compared directly.

Finally, the magnetic field strength at the surface of the EPID was measured with a THM1176 magnetometer (MetroLab Technology SA, Geneva, Switzerland) and the radius of the curvature of the scattered electrons was calculated for the peak and average energies.

Linearity of the EPID signal with dose in integrated images

The EPID response has been shown to deviate from linearity for short exposures, and this behavior becomes more pronounced for higher dose rates [113,114]. We investigated the linearity of the EPID dose response by delivering square fields of 20x20 cm^2 with different number of MUs (5, 10, 20, 50, 100, 200, 500, 1000 MU). Images were acquired with iViewGT in averaging mode, where the time-average of all acquired frames is recorded, along with a pixel factor which allows for the total signal to be calculated from the average image. A Farmer-type chamber was used simultaneously to record the linac output at the isocenter. The on-axis EPID pixel intensity was divided by the Farmer chamber value of each delivery to eliminate the effects of any fluctuation in the beam output, and the result was plotted as function of the number of MU and normalized to the 200 MU measurement. These measurements were performed for three dose rates (100%, 50% and 10% of 450 MU/min, the maximum dose rate) and each series was repeated three times.

Image lag in continuously acquired images

To study image lag in the EPID, the falling step response function (FSRF) was measured at maximum dose rate. Fields of 20x20 cm^2 were used and 1000 MU were delivered to reach equilibrium in the EPID signal. Frames were acquired until 100 frames after beam-off.

EPID response reproducibility

To study the short-term repeatability of the EPID response, an image was acquired every working day, over the course of 8 weeks. A field of 22x22 cm^2 field with 200 MU was used. At the same time, an IC measurement at the isocenter was performed to account for any fluctuations in the beam output.
For the IC measurement, a STARCHECK maxi MR ionization chamber

array (PTW, Freiburg, Germany) with 2 cm solid water buildup was used to measure the dose near d_{max} on top of the couch inside the bore of the MR-linac, at 153.5 cm from the source. Both the central value of the STARCHECK and the averaged on-axis region of the EPID image were normalized to the 10x10 cm^2 value of each measurement and the EPID values were divided by the IC ones.

3.3. Results

EPID relative position and MRI scanner

The displacement of the EPID was calculated to be 5.6 cm in the cranial direction at the EPID level, meaning that fields exceeding 8.1 cm in the cranial direction at isocenter plane cannot be completely detected by the EPID since part of the beam falls outside the panel.

Behind the parts of the beam that are shielded by the gradient coils, the attenuation was found to be up to 47% larger than on the beam axis, affecting only beams larger than 4.8 cm in both the cranial and caudal directions of the longitudinal axis.

The non-centered position of the panel and the strongly attenuated parts of the beam travelling through the gradient coils of the MRI can be seen in **Figure 3.2** where EPID images acquired with a large square field on the MR-linac and a conventional linac are compared.

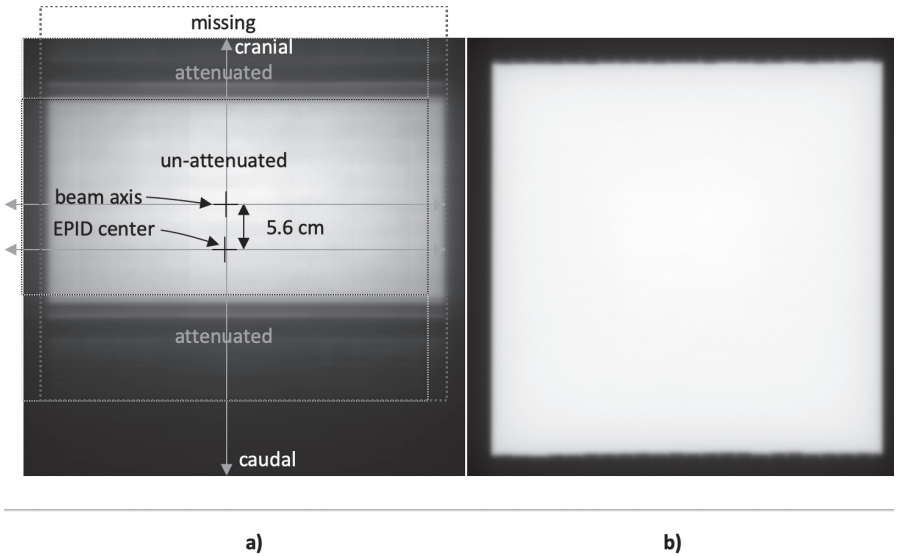

Figure 3.2. a) EPID image of a 20x20 cm^2 (FFF) beam, acquired on the MR-linac system. The centers of the EPID and the beam are marked with a cross and a dashed line shows the entire square shape of the field arriving to the EPID, which the EPID receives in un-attenuated parts (like in conventional linacs), attenuated parts, and missing parts. **b**) EPID image of a 23x23 cm^2 beam in a conventional linac (with flattening filter). Note that, for the sake of visual comparison, the field sizes at isocenter differ in order to receive an effective field of approximately 36.8 cm^2 at the EPID level in both cases.

The mechanical flex of the EPID in the MR-linac was found to have a largest deviation of 0.6 mm in the left-right direction and 0.2 mm in the cranial-caudal direction. This is a smaller deviation than in conventional linacs, where the average of the largest deviations are 1.3 mm and 1.6 mm respectively, probably because the EPID in the MR-linac is mounted on a ring allowing for minimum movement.

EPID response to scatter from the MRI scanner

In the MR-Linac (with the magnetic field activated), the EPID central area pixel intensity as a function of field size, presented in **Figure 3.3,** shows a different response compared to the microDiamond detector measurements at the EPID level (same SDD). For direct comparison,

EPID and microDiamond relative outputs acquired at a conventional linac are also plotted, showing closer agreement with each other. A ratio of the microDiamond measurement to the EPID signal output is shown for the MR-Linac and the conventional Linac.

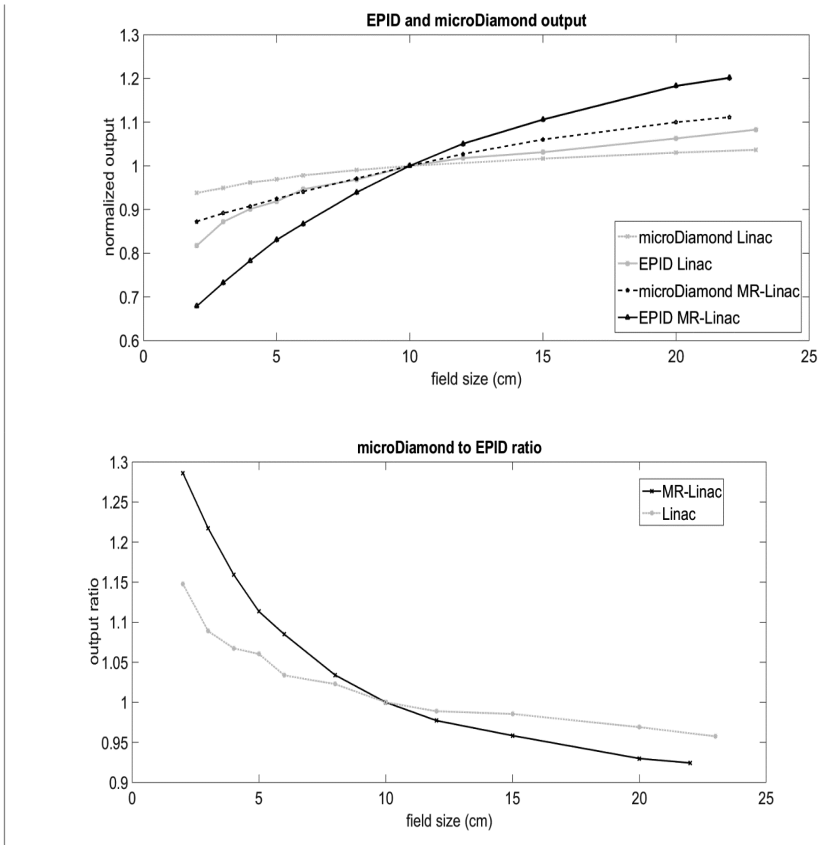

Figure 3.3. **a**) Field size dependence of microDiamond detector measurements at the EPID level (dashed line) and averaged EPID signal over the central 10x10 pixels (solid line) for the MR-linac system (black) and a conventional linac (grey); **b**) the output ratio of the microDiamond detector to the EPID signal is plotted for both the conventional linac (dashed grey) and the MR linac (solid black).

In the MR-linac, the steeper curve of the EPID response, compared to the MicroDiamond detector signal, can be attributed to the higher

sensitivityof the EPID to low-energy scatter, resulting from the combination of electrons scattered from the MRI-housing and the small air gap.

In the MR-linac, the relative output of the EPID compared to the MicroDiamond detector ranged from -22.3% to 8.2%, whereas in a conventional linac it ranged from -12.9% to 4.4% for field sizes of 2x2 and 22x22 cm^2 respectively.

Angular dependence of the beam attenuation at isocenter and EPID level

In **Figure 3.4. a**), an experiment performed with the magnetic field activated, shows the output of the beam measured at the isocenter with an IC (black) in a cylindrical phantom for a 10x10 cm^2 square field. In grey, the averaged signal from the central region of the EPID images is plotted. The curves are normalized at the 90 degrees gantry angle, where the beam does not traverse the treatment couch for the two measurements.

Figure 3.4. b) shows a polar plot of the ratio of the IC/EPID readings as a function of the gantry angle indicating that there is a varying attenuation between the isocenter and the EPID. Note that in both graphs the region between 7 to 20 degrees is omitted, since irradiation is prohibited due to the presence of a pipe, at 13 degrees. In **Figure 3.4. a**) and **b**) the attenuation of the pipe is clearly apparent as a drop in EPID signal for gantry angles around 193 degrees.

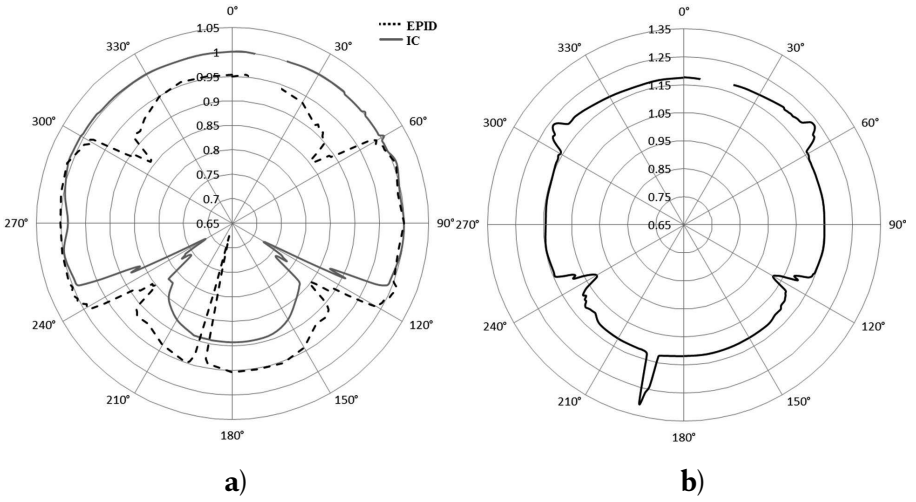

Figure 3.4. a) The output factor at the isocenter (solid-grey) and at EPID level (dashed-black) as function of the gantry angle and normalized to the measurement at 90 degrees. **b**) The normalized ratio of IC/EPID.

Drops in the EPID measured output at gantry angles 55, 120, 240 and 305 are related to structures of the couch attenuating the beam un-uniformly on its path towards to EPID. The output factor measured at the isocenter only reflects the attenuation at gantry angles 120 and 240, when the couch structures are irradiated before reaching the detector at isocenter.

EPID response with and without the magnetic field

The magnetic field measured on the surface of the panel did not exceed 10 mT, yielding an electron trajectory radius of 2.2 m for a peak energy of 6 MeV, and of 0.84 m for an average energy of 2 MeV. **Figure 3.5** shows the normalized relative profiles of EPID images acquired when a 20 cm thick slab phantom was irradiated with square fields with and without the magnetic field. More than 99% of points show local deviations smaller than 3%. 2D γ-analysis (local, 2%, 1 mm, 20%) reported an average value of γ_{mean} of 0.15 ± 0.06 (1SD) and an average γ pass rate of 98.6% ([98.0, 99.1], 95% CI).

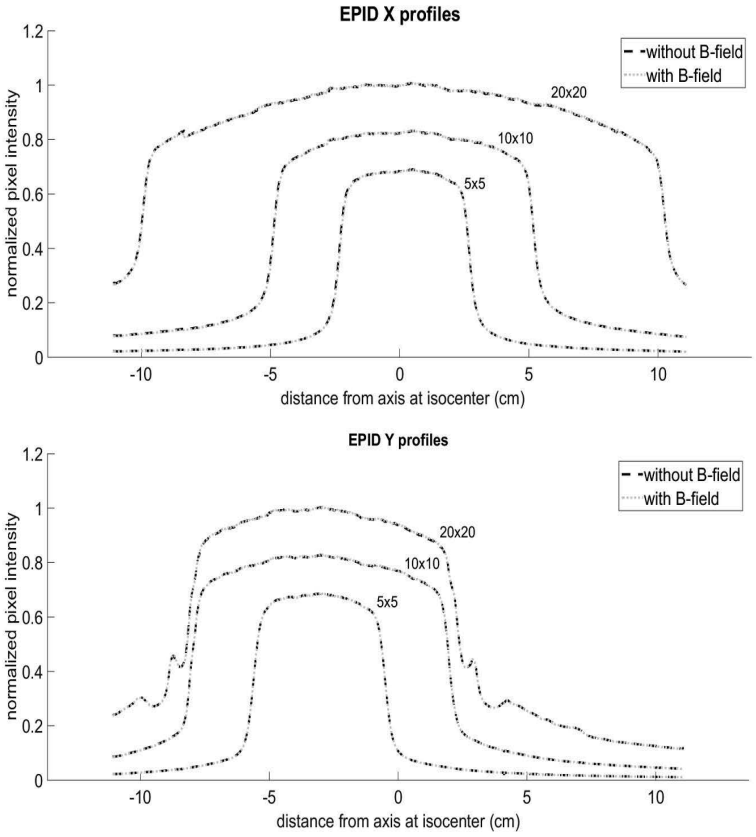

Figure 3.5. X (top) and Y (bottom) EPID lateral profiles of square fields irradiated with 5x5, 10x10 and 20x20 cm^2 to a 20 cm slab phantom are shown for images acquired with (dotted-grey) the magnetic field, and without (dashed-black). Note the shift of the Y profiles due to the non-centered position of the EPID, as well as the strong attenuation because of coils affecting the 10x10 cm^2 curve in the penumbra, and more clearly the 20x20 cm^2 field, creating also oscillations due to heterogeneities in the cryostat, and the ring.

Linearity of the EPID signal with dose in integrated images

With the magnetic field activated, the relative response of the panel, calculated as the EPID signal divided by the corresponding IC value, is plotted against the delivered MUs, normalized to 200 MU (**Figure**

3.6. a)). Also included is the data from a measurement performed on a conventional linac. Variations in the EPID response are within 4% for the MR-linac. This is similar to previously published results in conventional linacs [137,138] and comparable to other panels at our department that are currently used for *in vivo* dosimetry. In **Figure 3.6. b**) the relative EPID response at different dose rates is plotted. The best linearity is observed at lower dose rates.

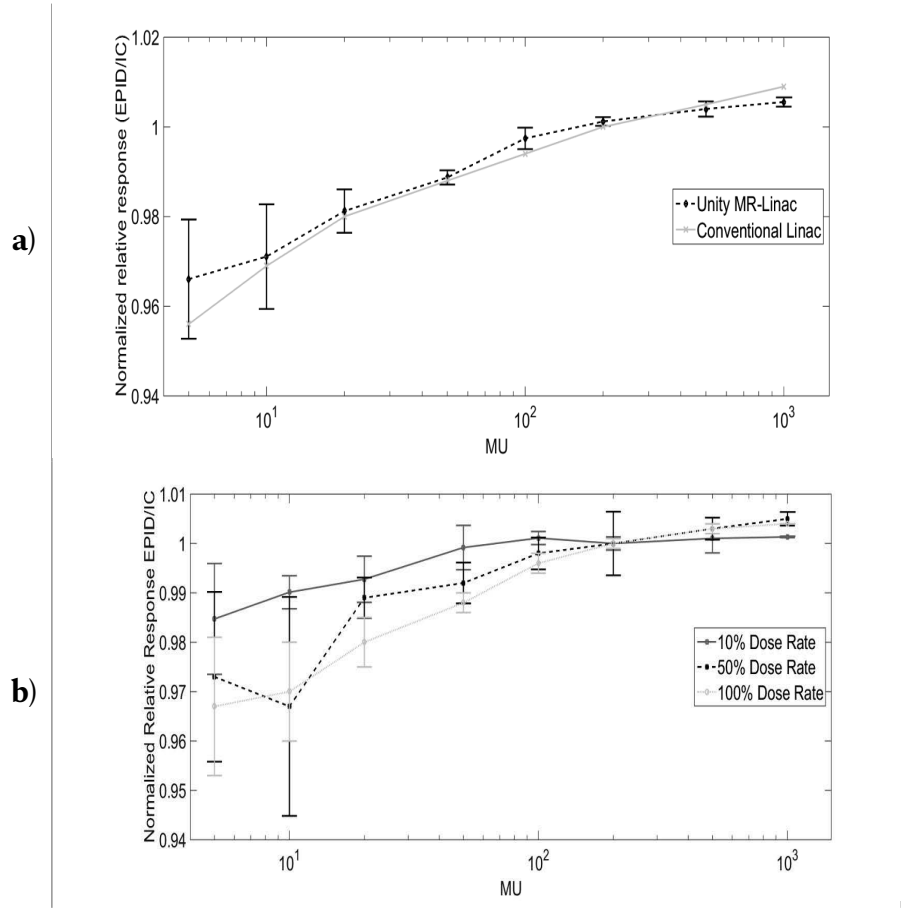

Figure 3.6. a) The relative EPID response (EPID/IC) as a function of dose for a varying number of MUs is plotted for the MR-linac (dashed-black) and in a conventional linac (solid-grey), normalized to the 200 MU point. Variations of the EPID signal divided

by the IC measurement are found within 4% at low MUs for the MR-linac. When compared to the same experiment performed at a conventional linac with the same model panel, deviations were within 5%. **b**) The relative EPID response (EPID/IC) as a function of dose for the MR-linac, normalized to the 200MU point, for 100% dose rate (dotted-light grey), 50% (dashed-black) and 10% (solid-dark grey). Error bars show the standard deviation of 3 measurements.

Image lag in continuously acquired images

Measuring the falling step response function (FSRF), after the beam at equilibrium was turned off, the EPID signal dropped below 2% of equilibrium value after 0.6 seconds (2 frames) and below 1% after 2 seconds (or 7 frames).

EPID response reproducibility

The ratio of the daily EPID and ionization chamber output was normalized to the average ratio measured over 8 weeks. A standard deviation of 0.5% (1 SD) was found, comparable to other EPID studies in conventional linacs [119].

3.4 Discussion

We have studied the dosimetric characteristics of the a-Si panel in the Elekta Unity machine and pointed out the challenges and limitations towards its use in dose verification applications.

A main drawback of the current setup is that parts of fields exceeding 8.1 cm in the cranial direction at isocenter will not be able to be verified with the EPID due to the non-centered position of the panel. The consequences of this EPID displacement will vary depending on the solution to be used. For *in vivo* EPID dosimetry in 3D, transit EPID patient images are typically used to reconstruct the 3D dose distribution within the patient whether using a back-projection algorithm or by

estimating the energy delivered fluence by the accelerator and then using it as input to a dose engine for a forward dose calculation. In these solutions, the EPID images of large fields will miss parts of the beam and this will lead to wrong reconstructions. For these large fields though, *in vivo* dose verification in 2D (or point dose) may still be possible by using back-projection algorithms on the available part of the beam or by using other transit EPID-dosimetry solutions such as predicted portal image methods. In all cases, an automatic position correction of the EPID images to the center of the beam has to be introduced for EPID dosimetry at a pre-processing stage.

The relative signal of the EPID, for increasing field sizes, compared to the relative output of a microDiamond detector measuring on top of the EPID, confirms the over-sensitive response of the panel compared to the chamber, suggesting a large amount of scatter, originating in the MRI housing and reaching the EPID. When EPID images are used for dosimetry, a correction for the MRI to EPID scatter must be applied after the raw image is processed. Moreover, although the definitive version of the couch is expected to differ from the current design, we showed that the attenuation of the beam between the isocenter and the EPID is not homogenous for the entire image, since couch structures and the MRI gradient coils cause extra attenuation as the beam traverses them. Additionally, this attenuation has been shown to be gantry angle dependent, suggesting that any correction applied to correct for scatter and attenuation through the MRI scanner would also have to be gantry angle dependent. A proof of concept for an adaptation of a back-projection algorithm to account for the presence of the MRI scanner between the isocenter and the EPID is investigated in [139]. The EPID signal in Figure 4 is, withal, less modulated with rotation than the IC output due to scattered photons that the EPID receives from the MRI scanner, therefore the attenuation factor should be determined after the scatter from the MRI scanner has been subtracted. However,

the use of the EPID for predicted portal images would not require the correction for scatter and attenuation from the MRI scanner, but only a characterization of the EPID response.

The low field strength and calculated radius of curvature of electrons at the level of the EPID suggested that any effect of the magnetic field on the EPID images would be negligible. This was confirmed in this study with EPID images acquired without the magnetic field. In other words, no additional refinements are required for the dose modelling of the EPID in the MR-linac due to the presence of a magnetic field. The magnetic field will have to be accounted for in *in vivo dose* reconstructions, of course. This could be achieved by using the log files of the linac to estimate the delivered fluence by the accelerator and then using it as input to a dose engine that accounts for magnetic field effects in its forward dose calculations. Back-projection algorithms are not capable of correct for the presence of magnetic fields. An alternative would be to compare the reconstructed dose to a new plan in the TPS, calculated without the magnetic field just for verification purposes (a 'non-magnet' solution, similarly to the 'in-aqua' concept for lung cases [86]). Alternatively, a back-projection of the EPID images to obtain the primary fluence in front of the patient could be used to feed a Monte Carlo simulation accounting for the magnetic field effects, and to be compared to the planned dose distribution from the TPS.

The linearity of the EPID response with dose was shown to be comparable to that of other panels in our department. The similarity between the results for the detector in the MR-linac and in a conventional linac suggests that dose linearity and dose rate dependency do not compromise the dosimetric performance of the panel in Elekta's MR-linac.

The accuracy achieved by an EPID dosimetry solution in the MR-linac remains to be seen when the challenges listed in this paper have been addressed.

3.5. Conclusion

The study of several characteristics of the EPID and its use for dosimetric applications suggests that the magnetic field, the dose rate dependency, and dose linearity have similar results compared to experiments performed in conventional linacs. However, the implementation of in vivo transit EPID dosimetry solutions will have to address the challenge of the panel position and include gantry angle-dependent corrections for both the attenuation of the beam and the scatter from the MRI housing.

3.6. Disclosure of conflicts of interest

Support for this research was provided, in part, by Elekta AB, Stockholm, Sweden.

3.7. Acknowledgments

We would like to thank Jochem Kaas, Thijs Perik, Begoña Vivas and Robert Spaninks for assistance with the measurements.

3